Effect of alloying elements on thermal stability of Aluminium-Cerium based alloys

Dheeraj Kumar Saini (dks12@iitbbs.ac.in)
Indian institute of Technology Bhubaneshwar India
Rahul Gope
Indian Institute of Technology Bhubaneshwar India
Animesh Mandal
Indian Institute of Technology Bhubaneshwar India

Research Article

Keywords: Al-Ce alloys, Heat treatment, Microhardness, Intermetallic, Casting

Posted Date: March 30th, 2022

DOI: https://doi.org/10.21203/rs.3.rs-67587/v3

Effect of alloying elements on thermal stability of Aluminium-Cerium based alloys

D. Saini[a, b*], R. Gope, A. Mandal[a]

[a]School of Minerals Metallurgical and Materials Engineering, Indian Institute of Technology Bhubaneshwar, India

[b]Department of Mechanical and Industrial Engineering, Indian Institute of Technology Roorkee

Keywords: Al-Ce alloys, Heat treatment, Microhardness, Intermetallic, Casting

1. Introduction

Aluminium alloys are desirable for automotive and aerospace industries due to their lightweight, outstanding castability and excellent mechanical properties. These alloys can be used as a replacement in the automotive sector with currently used iron-based alloys and titanium alloys wherever suitable. The high strength-to-weight ratio of aluminium alloys lead to better fuel economy and help reduce greenhouse gases. Besides, aluminium alloys tend to make a robust passivizing protective oxide layer that makes it corrosion resistant. One of the major drawbacks of aluminium alloys is that it does not retain their mechanical properties at higher temperatures. The addition of rare earth elements to aluminium alloys can fill this gap. In this context, recent studies on Al-Ce alloys show improved design efficiency for the transport industry and better mechanical properties for high-temperature applications. At the hyper eutectic point, Al-12Ce alloy contains a eutectic mixture of Al and $Al_{11}Ce_3$ intermetallic. This $Al_{11}Ce_3$ present in aluminium matrix is metastable and does not respond to heat treatment. In the lanthanide series, earlier lanthanides up to Sm form $Al_{11}RE_3$ (RE refers to rare earth) intermetallic and later lanthanides from Eu form Al_3RE phase that is stable in aluminium matrix. In the Al-RE system, thermodynamically stable Al_3RE phase precipitates out during solidification and no further heat treatment is needed for Al_3RE precipitation [1]. Al-Ce alloys are castable for a wide range of Ce contents and compatible with available casting infrastructure.

Addition of Mg to Al-Ce binary alloy allows precipitation of intermetallic phase during heat treatment and ensures better properties than previously developed binary Al-Ce alloys. The addition of Si in Al-Ce-Mg alloys has a negative impact on the castability of Al-Ce alloys and creates a flaky type CeAlSi intermetallic that adversely affects the mechanical properties. Sims et al. have found that a lower amount of Si addition to Al-Ce based alloys does not degrade the castability of alloys and provides better wear resistance at room temperature [2]. It was found that the addition of Ce up to 12 wt. % into Al increases the mechanical properties of a binary system (Figure1) [3]. To develop reasonable room temperature and high temperature (400 °C) strength, other alloying elements (Si, Mg and Cu) were added to binary Al-Ce alloys. Hu et al. characterize the Al-Ce-Mg alloy. This alloy manufactured by using the high pressure die casting. Addition of Mg does not form an intermetallic which constitute the Mg element. Mg addition causes the lattice distortion of Al thereby providing the solid solution strengthening [4]. Wu et al. investigate the creep resistance, ambient temperature strength and thermal stability of the Al-Ce-Ni alloy. They reported that high volume fraction of

intermetallic $Al_{11}Ce_3$ and Al_3Ni contribute to the higher strengthening at room temperate compared to Al-Ce alloy and provide creep resistance at 300-350 °C for prolonged period [5]. Figures 1 and 2 represent the summary of mechanical properties of Al-Ce based alloys available in the literature. Previous studies on binary Al-Ce alloys show improved thermal stability at high temperatures for various applications.

Therefore, the main objective of the present work is to understand the effect of alloying elements and correlate the microstructure-hardness-thermal stability of Al-Ce based alloys. This paper reports the effect of Si, Mg and Sr additions on the thermal stability of near eutectic Al-12Ce alloy. Microhardness variation was used to discuss the thermal stability of the Al-Ce based alloys. Typically, thermal stability is related to microstructure. The size, length scale, aspect ratio, orientation of eutectic, presence of intermetallic phases affects the thermal stability of the alloy. The size of eutectic and fine intermetallic phases depends on the cooling rate which determines the microstructure. A fine intermetallic also works as the precipitate by hindering the dislocation. Therefore, a combined study of hardness and microstructure can be used to analyse the thermal stability of the proposed alloy. A microstructural and hardness analysis was also elaborated by the Wu et al. for Al-Ce-Ni alloy [5].

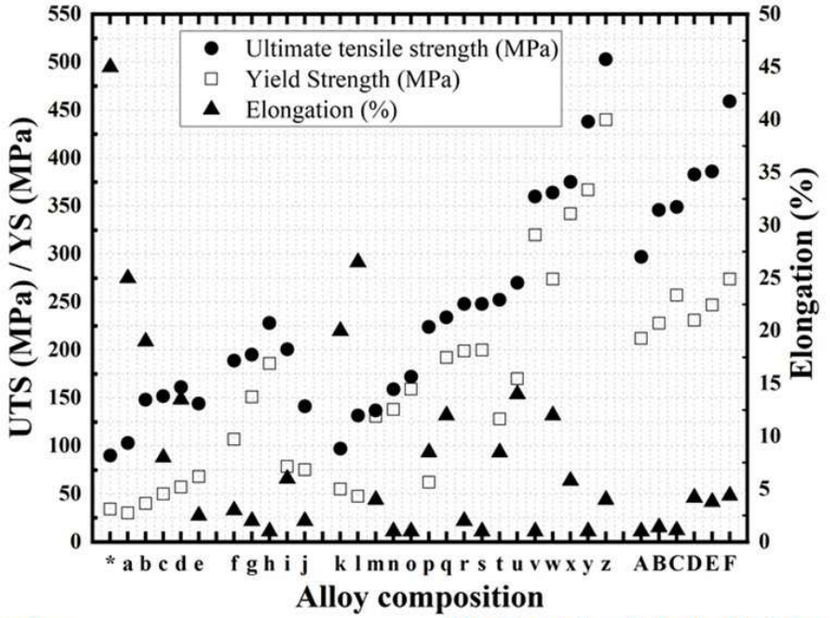

Binary alloys

* CPAl
a Al-6Ce
b Al-8Ce
c Al-10Ce
d Al-12Ce
e Al-16Ce

Ternary alloys

f Al-8Ce-4Mg
g Al-8Ce-7Mg
h Al-8Ce-10Mg
i Al-12Ce-0.4Mg
j Al-12Ce-4Si-0.4Mg

3D Printed alloys

A Al-3Ce-7Cu (As Printed, annealed at 300 °C for 1 h, Z direction)
B Al-3Ce-7Cu (As Printed, annealed at 200 °C for 3 h, Z direction)
C Al-3Ce-7Cu (As Printed, Z direction)
D Al-3Ce-7Cu (Printed, annealed at 300 °C, 1 h, XY direction)
E Al-3Ce-7Cu (Printed, annealed 200 °C, 3 h, XY direction)
F Al-3Ce-7Cu (As Printed, XY direction)

Heat treated and plastically deformed alloys

k Al-8Ce-10Mg (annealed at 315 °C for 0.5 h
l Al-12Ce (T6 Heat Treated)
m Al-8Ce-10Mg (annealed at 260 °C for 0.5 h)
n Al-8Ce-10Mg (annealed 260 °C for 336 h)
o Al-8Ce-10Mg (annealed at 315 °C for 216 h
p Al-12Ce-0.4Mg (T6 Heat Treated)
q Al–7Ce –14Cu (wrought, cold rolled annealed 350 °C for 3 h)
r Al-8Ce-4Mg (T4, stepped Homogenization)
s Al-8Ce-10Mg (T4 Heat Treated)
t Al-12Ce-4Si-0.4Mg (T6 Heat Treated)
u Al–7Ce –14Cu (wrought, hot rolled annealed at 350°C for 3h)
v Al–7Ce –14Cu (wrought, hot rolled)
w Al-8Ce-10Mg (cast, Extrusion 52:1)
x Al-8Ce-10Mg (cast, Extrusion 5:1)
y Al–7Ce –14Cu (wrought, cold rolled)
z A20X®T7 Commercial alloy [www.aeromet.co.uk]

Figure 1: Mechanical properties of Al-Ce alloys at room temperature [2,3,6]. In binary alloys, Al-12Ce shows better mechanical properties than other binary alloys. Mg increases UTS and YS in ternary alloys but simultaneously decreases % elongation. 3D printed alloys (manufactured by selective laser melting) show considerable improvement in mechanical properties compared to cast ternary alloys.

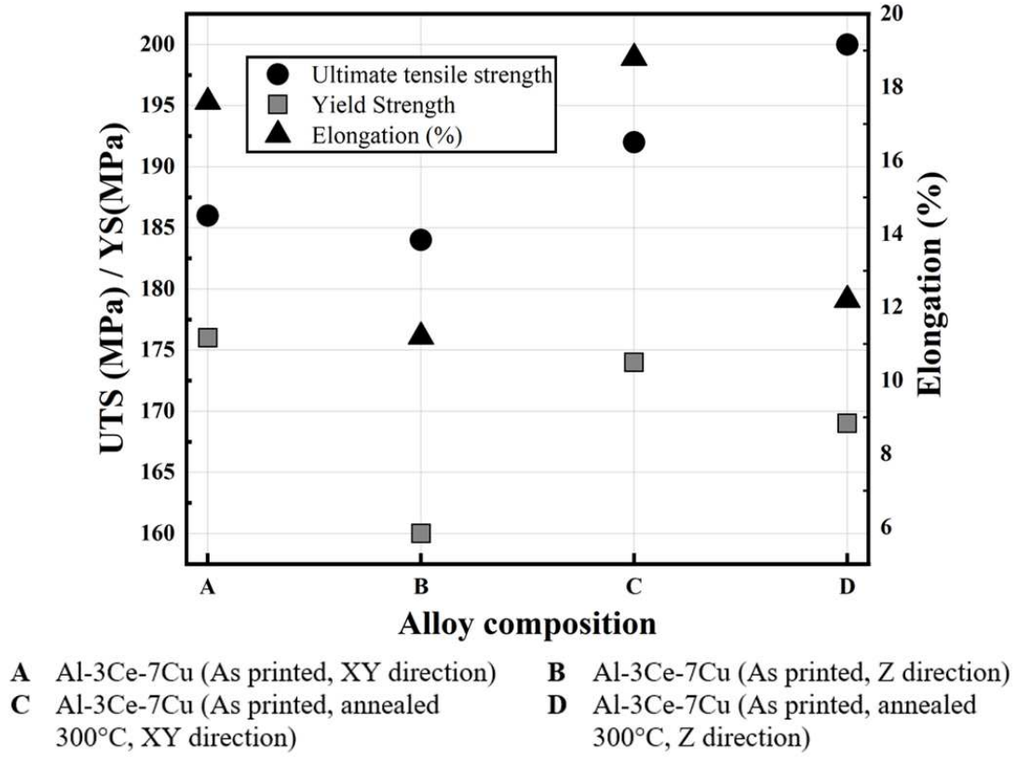

Figure 2: Mechanical properties of 3D printed (manufactured by selective laser melting) Al-Ce-Cu alloys measured at 250 °C [6].

2. Experimental details

2.1 Alloy preparation

Near-eutectic Al-Ce based alloys with the composition of Al-12Ce, Al-12Ce-4Si, Al-12Ce-0.4Mg, Al-12Ce-4Si-0.4Mg and Al-12Ce-4Si-0.4Mg-0.25Sr (wt. %) were cast for the present study. Commercial pure aluminium (CPAl) ingot and the following master alloys having purity level 99.7% were used as feedstock: Al-50Si, Al-20Ce, Al-20Mg, and Al-10Sr (wt. %). All the alloys were prepared using a resistance-type furnace (KANTHAL, SN 1015) and a clay bonded graphite crucible. Master alloys of Al-Ce, Al-Si and CPAl together were placed in a crucible and allowed to melt in a furnace held at 785 °C. Al-Mg and Al-Sr master alloy were added to the melt at the end with intermittent stirring to ensure chemical homogeneity and minimize oxidation loss. After complete melting, the alloy was degassed with a commercially available degasser, C_2Cl_6. The top oxide layer of the melt was skimmed off before pouring the molten alloy into a mild steel mould (1.5 cm diameter and 15 cm height), which was preheated at 300 °C in an air circulated oven. After casting, the cylindrical alloy bars were sectioned using the abrasive cutter to prepare a 2-3 mm thickness sample for metallography, heat treatment, and subsequent studies.

2.2 Metallography and microstructure characterization

For microstructural analysis, ASTM E3 standard metallographic practice was adopted, where final polishing was carried out using 0.01 μm colloidal silica. Keller's reagent was used for chemical etching whenever required. The FESEM (Field Emission Scanning Electron Microscope) was equipped with a backscattered electron (BSE) and a secondary electron (SE) detector. The attached energy dispersive spectroscopy (EDS) was used for phase-specific chemical analysis with 5 kV and 20 kV acceleration voltages. Phase-specific EDS analysis was carried out on three random locations for each phase and average composition was calculated. For heat treatment studies, samples were polished using alumina slurry up to 12-13 μm surface roughness. Image analysis was carried out using Image J software (version 1.53b) and the systematic manual point count method (ASTM E562) was used to calculate the volume fraction of phases. X-ray diffractometer was equipped with a solid-state detector and operated using Cu-K_α radiation. Quantification of phases and XRD pattern was analyzed using Xpert high score (3.0.0) software.

3. Results and discussion

3.1 Al-12Ce alloy

Binary Al-12Ce (Figure 3a) alloy shows the presence of Al (light grey in the matrix) and intermetallic $Al_{11}Ce_3$. The alloy shows a fine faceted eutectic mixture of Al and lathe like intermetallic $Al_{11}Ce_3$. This eutectic mixture can be referred to as eutectic colonies [7]. Figure 3b shows the XRD pattern of as cast and selected heat-treated alloys. The XRD pattern confirms the presence of Al and $Al_{11}Ce_3$ phases, also confirmed by the previous studies [8,9]. Based on the hardness variation, some critical points were selected from the heat treatment chart and compared with cast alloy. These critical points are encircled in figure 4c. The XRD pattern reported in figure 3b shows the repeated pattern at a different time and temperature ranges on the critical points. The consistency in the XRD pattern and the peak intensity indicates the retaining of the phases at all the selected temperature ranges.

Figure 4a shows the $Al_{11}Ce_3$ intermetallic phase treated at 300°C for 10 hours, which seems to have spheroidized at many regions and become less intertwined than small and entangled laths in as cast alloy mentioned in figure 4a. Heat treatment at 300°C for 10 hours results in a eutectic microstructure undergoing minor morphological changes. Spheroidization in heat treated microstructure results in a localized minimization of micro constituent surface energy at the eutectic through surface diffusion within the intermetallic rather than bulk diffusion through the matrix [9]. In a cast condition, the volume fraction of $Al_{11}Ce_3$ was found to be 15.5 ± 1.2 %, as determined using the systematic manual point count method. The volume fraction of $Al_{11}Ce_3$ increased from 0.15 to 0.18 upon heat treatment at 300 °C for 10 hours. This indicates the gradual change in phase fraction of intermetallic with time and temperature. Strong vacancy binding of Al to Ce atoms decreases the degradation of $Al_{11}Ce_3$ intermetallic and therefore reduces vacancy diffusion (the dominant transport mechanism for solute atoms within the matrix) [10,11]. The intermetallic is trapped by the zero solubility of Ce in the aluminium matrix. This trapping prevents the system from minimizing surface energy through diffusion, which prevents the alloys from coarsening. So, low solubility and a large atomic size difference between Ce (1.81 Å) and Al (1.43 Å) result in a low diffusion coefficient compared to other alloying elements. As an

illustration, the diffusion data for Al, Ce and other solutes in Al were calculated using the data available in the literature (Table1).

Figure 4c shows the hardness study for heat treated binary Al-Ce alloys at a temperature of 200 °C, 300 °C and 400 °C for up to 100 hours. Al-12Ce shows microhardness of 510 ± 36.29 MPa compared to 200 MPa for pure Al [12]. The increased hardness from as-cast to heat treated condition for 300 °C up to 10 hours can be approximated by Orowan strengthening.

Microstructure quantification

An attempt was made to understand the strengthening mechanism in Al-Ce based alloys. Among the Al alloys, the primary strengthening mechanisms are solid solution strengthening, hall-petch hardening, and precipitation hardening. Orowan described that precipitation strengthening is a result of precipitate-dislocation interaction in the matrix leading to the formation of dislocation loop around the precipitate and an increase in yield strength of the material is given by [13]

$$\Delta\sigma = M.\frac{0.4 * G * b}{\pi\sqrt{(1-\nu)}}.\frac{\ln(\frac{2\bar{R}}{b})}{\lambda} \quad (1)$$

Where M: Taylor factor of the matrix, G: Shear modulus of the matrix, ν: Poisson ratio of the matrix, b: magnitude of Berger vector, $\bar{R}$: mean planar precipitate radius given by:

$$\bar{R} = \frac{\pi}{4} * (R) \quad (2)$$

Where R: mean precipitate radius

$\bar{R}$ and λ depends on the distribution of precipitates where λ is the effective inter-precipitate distance. For mono dispersed assembly, these are given by [14–16]**:**

$$\lambda = \left(\sqrt{\frac{2\pi}{3f}} - \frac{\pi}{2}\right) * (R) \quad (3)$$

Where f: precipitate volume fraction

The parameters for aluminium in equation 1are as follows: M=3.06, ν=0.345 [17], b=0.286 nm and G=25.4 GPa [18]. By using equations 1, 2 and 3, increase in Orowan strength for as cast and heat-treated condition (300 °C for 10 hours) was estimated to be ∼53.07 MPa and ∼42.27 MPa that is significantly lower than the experimentally measured (ΔHV/3) values of ∼103.37 MPa and ∼112.52 MPa respectively (Table 2). Here ΔHV/3 is approximated as the increment in strength and defined as the difference in microhardness values of as-received alloy and pure Al [19]. The disparity is calculated and measured values are explained by Sims et al. [9]. The neutron diffraction study showed that the load transfer mechanism played a significant role in improving the strength. Orowan strengthening and load transfer mechanisms are expected to be active at higher temperatures, although less efficient than at ambient temperature, as

dislocation can climb to bypass $Al_{11}Ce_3$ precipitate, and the fast-creeping Al matrix transfers less load to $Al_{11}Ce_3$ precipitate [9]. An increase in the mean diameter of $Al_{11}Ce_3$ from 142 ± 26 nm in cast alloy to 175 ± 21 nm in heat treated alloy at 300 °C for 10 hours was observed (Figure 4a and b). Although there was a minor coarsening after heat treatment at 300 °C for 10 hours (Figure 3d), Orowan strengthening still dominated in the heat-treated alloy due to an increase in volume fraction of intermetallic (equation 1) [7]. The hardness values show a peak for all temperatures studied and then stabilized on prolonged heat treatment for up to 100 hours. Thus, a combination of low Ce solubility in the Al matrix and low Ce diffusion coefficients avoids coarsening mechanisms through Ostwald ripening, while the high thermodynamic stability of the $Al_{11}Ce_3$ intermetallic resists substantial microstructural evolution in the Al-Ce alloys and, by extension, degraded mechanical properties. This demonstrates that both the hardening mechanisms were active at room and elevated temperatures. This study shows the ageless behavior of intermetallic $Al_{11}Ce_3$ after heat treatment, supported by Stromme et al. [20].

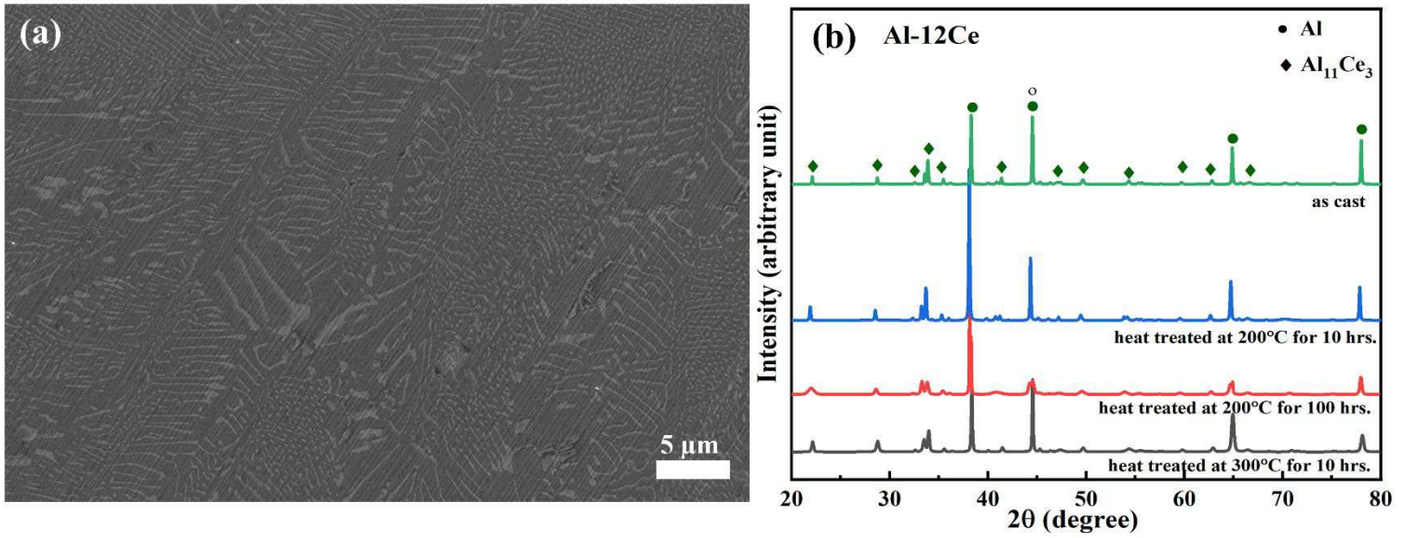

Figure 3: FESEM micrograph of as-cast Al-12Ce (wt. %) alloy showing (a) lathe like intermetallic $Al_{11}Ce_3$ showing primary $Al_{11}Ce_3$, (b) XRD pattern

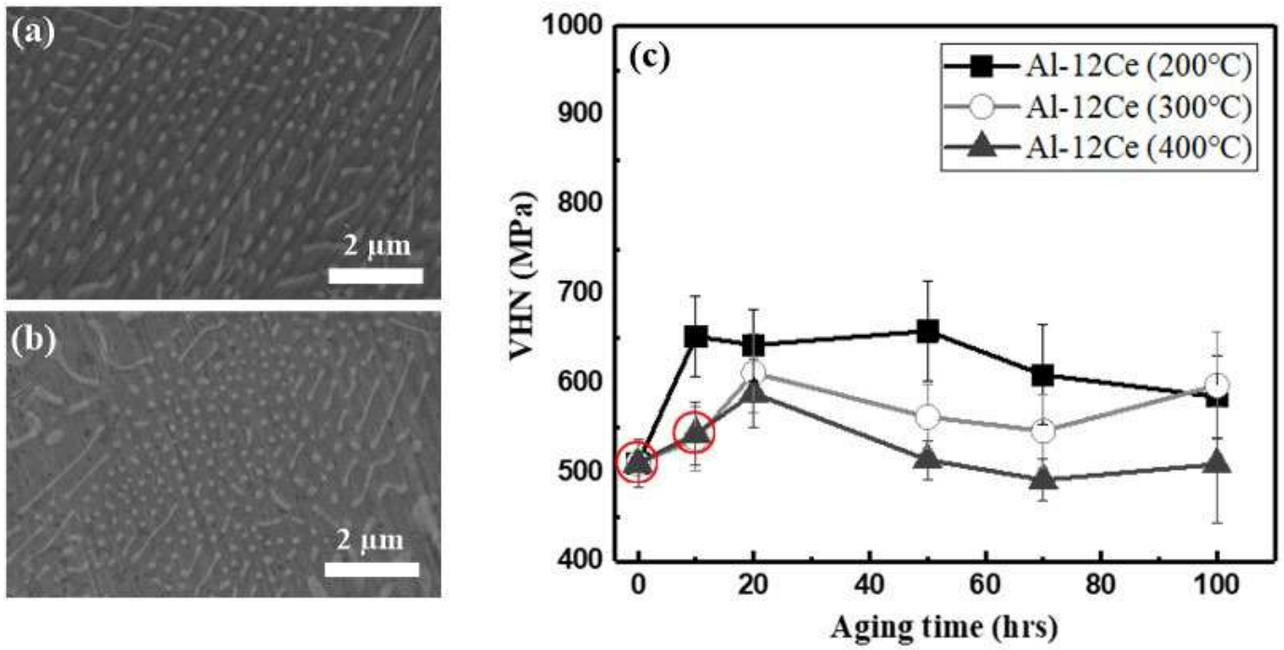

Figure 4: FESEM micrograph for Al-12Ce (wt.%) alloy (a) as-cast state shows the globular form of intermetallic in Al matrix (b) spheroidization and coarsening of intermetallic at 300 °C after 10 hours of heat treatment (c) Heat treatment of Al-12Ce alloy up to 100 hours for different time intervals (0, 10, 20, 50, 70 and 100 hours

Table 1: Measured diffusion data for elements (solutes) in Al used in the present study [11,21]

Element	Pre-exponential $D°(m^2s^{-1})$	Activation Energy, Q (KJ/mole)	D at 200 °C (m^2s^{-1})	D at 300 °C (m^2s^{-1})	D at 400 °C (m^2s^{-1})
Al	1.37×10^{-5}	124.0	2.77×10^{-19}	6.79×10^{-17}	3.25×10^{-15}
Ce	1.90×10^{-10}	111.0	1.04×10^{-22}	1.47×10^{-20}	4.60×10^{-19}
Mg	1.49×10^{-5}	120.5	7.33×10^{-19}	1.54×10^{-16}	6.61×10^{-15}
Si	1.38×10^{-5}	117.6	1.42×10^{-18}	2.62×10^{-16}	1.02×10^{-14}

Table 2: Calculated increase in strength by Orowan/load transfer mechanism

Alloy	Total increment in strength (ΔHV/3) (MPa)	Orowan contribution (MPa)	Load transfer contribution (MPa)
Al-12Ce (as cast)	103.37	42.27	61.10
Al-12Ce (after 10 hours of heat treatment at 300 °C)	112.52	53.07	59.45

3.2 Al-12Ce-4Si alloy

The mechanical properties of Al-Ce alloys can be significantly improved by adding a small amount of Mg and Si shown by the Al-12Ce-4Si and Al-12Ce-4Si-0.4Mg. Cerium reacts favourably with Si and results in the formation of a new ternary tetragonal intermetallic AlCeSi confirmed by Sims et al. [9]. The solubility of Si in the Al matrix phase is 1.5 wt.% at high temperatures and it is possible to quench a supersaturated solids solution to 11 wt.%. The low mobility and reactivity of Ce lead to the immediate intermetallic formation. Figure 5a shows the microstructure of as-cast Al-12Ce-4Si comprises of α-Al, $Al_{11}Ce_3$ and AlCeSi phases. The presence of intermetallic phases $Al_{11}Ce_3$ and AlCeSi is also confirmed by the XRD pattern shown in figure 5b. Based on the hardness variation few critical points were selected for the Al-12Ce-4Si alloy encircled in figure 6b. XRD pattern at those critical points does not indicate the transformation of new phases (Figure 5b).

The needle-like phases (white/AlCeSi) persisted even after heat treatment at different temperatures and aging times (Figures 6a, b). This shows the high thermal stability of intermetallic phases in aluminum [22–25]. The effect of Si on yield strength appears to be inconsistent and affects the ultimate tensile strength and work hardening [20]. Therefore, Si addition in Al-12Ce alloy results in a marginal change in hardness compared to binary Al-12Ce alloy. Figure 6c shows the heat treatment studies for Al-12Ce-4Si alloy. After heat treatment at 200 °C for 10 hours, there is a significant increase in hardness. This could be due to the combined effect of dispersion strengthening, solid solution strengthening, and load transfer mechanism activated at this temperature. Diffusion data (Table 1) shows that the diffusion coefficient of Si at 400 °C is 10^4 times higher than 200 °C. Thus, diffusion time for Si at high temperature is much lower and strengthening due to the solid solution could be lowered. Though microstructural changes observed at 200°C and 400 °C were not significant (Figure 6a and b), a decrease in hardness at 400 °C after 10 hours of aging time was significant, suggesting poor thermal stability of the alloy. After slight fluctuation, hardness became constant at all temperature ranges. It concluded the thermal stability of $A_{11}Ce_3$ and AlCeSi phases at elevated temperatures.

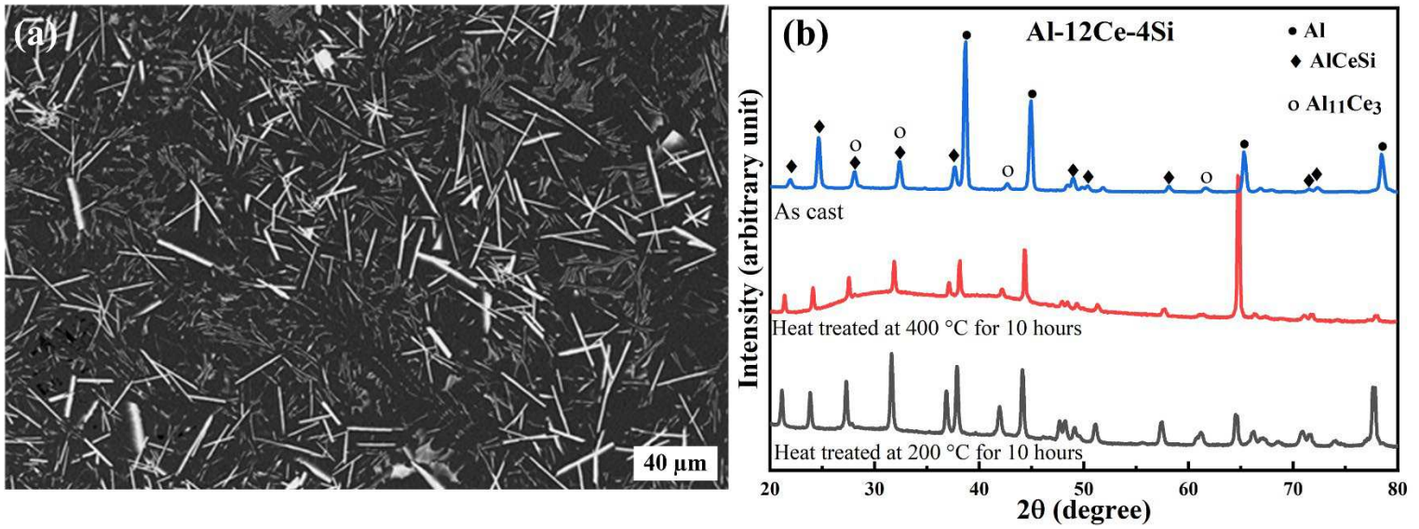

Figure 5: (a) FESEM micrograph of as-cast Al-12Ce-4Si (wt.%) alloy showing homogeneous distribution of eutectic mixture of $Al_{11}Ce_3$ and Al (b) XRD pattern of as cast and heat-treated alloy

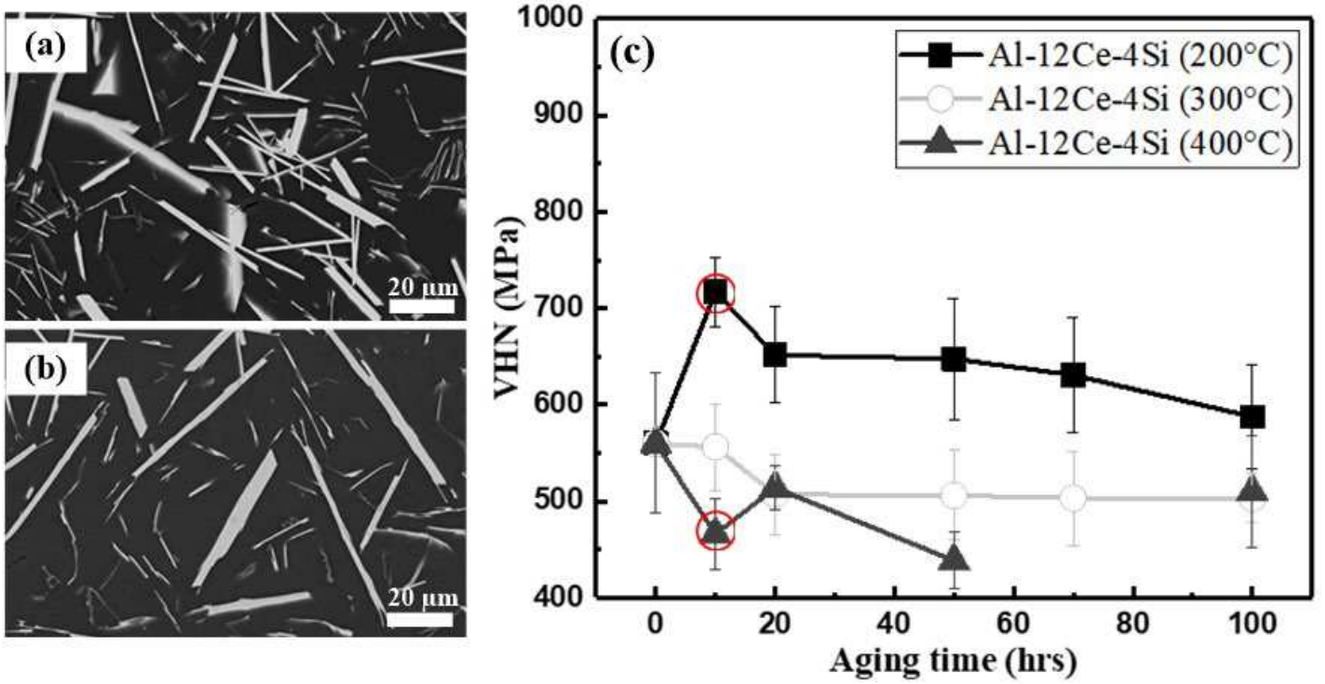

Figure 6: FESEM micrograph for Al-12Ce-4Si (wt.%) alloy in(a) heat treated condition at 200 °C after 10 hours (b) heat treated condition at 400 °C after 10 hours (c) Heat treated Al-12Ce-4Si alloy up to 100 hours for different time intervals (0, 10, 20, 50, 70 and 100 hours)

3.3 Al-12Ce-0.4Mg alloy

Figure 7a shows the as cast microstructure of Al-12Ce-0.4Mg alloy containing a eutectic mixture of Al and $Al_{11}Ce_3$ in which $Al_{11}Ce_3$ lathes are firmly interlinked. However, the microstructure also shows the primary cubic crystal of Al_3Mg_2, which was shown by the XRD pattern in figure 7b. The presence of these phases is also supported by Weiss

et al.[8]. They found that the presence of large primary crystal of Al_3Mg_2 decreases the elongation of Al-12Ce alloy more than 50 % compared to Al-12Ce binary alloy.

Microstructure Quantification

Figures 8a and c show the microstructure of the heat-treated samples at 400 °C and 200 °C, respectively, followed by the different aging times. Lathe-like interconnected $Al_{11}Ce_3$ transforms into discrete particles after heat treatment at 400 °C for 10 hours and becomes more globular than heat treatment at 200 °C for 100 hours (Figure 8c). These alloys showed a 23% increase in hardness at 200 °C for 100 hours, while at 400 °C, there was a 10% decrease in hardness compared to the cast condition (Figure 8b). The variation in the hardness can be inferred from solid solution strengthening, Orowan strengthening and load transfer mechanism. To find the contribution of Orowan strengthening microstructural study was conducted on the critical point. Table 3 shows that the aspect ratio of $Al_{11}Ce_3$ decreases at 400 °C compared to 200 °C. The difference in diffusivity of 3-4 orders (Table 1) between 200 °C and 400 °C explains the extent of fragmentation at two temperatures. The increment in Orowan strength for heat-treated alloy at 200 °C for 100 hours and 400 °C for 10 hours was calculated to be ∼15 MPa and ∼18.8 MPa that is significantly lower than experimentally measured (ΔHV/3) values of ∼179.23 MPa and ∼132.80 MPa respectively (Table 3). This suggests that the strength increase was primarily due to solid solution strengthening and load transfer capability of a matrix to the intermetallic. The decrease in hardness at 400 °C after 10 hours of heat treatment can be inferred to loss of solid solution strengthening due to the release of strain energy. At high temperatures, fragmentation of $Al_{11}Ce_3$ lathes leads to the inactivation of the load transfer mechanism and could be the possible reason for the decrees in hardness. It was difficult to quantify the individual contribution of solid solution strengthening and load transfer mechanisms due to the formation of new phases during heat treatment. Increasing the heat treatment time beyond 50 hours does not show the significant decreasing pattern of the hardness except 400 °C. In the case of 200°C and 300°C, the variation in hardness after 50 hours of aging almost becomes constant. This study shows the thermal stability of the retained phases with hardness variation.

The purpose of incorporating Mg into a binary alloy was to alter the microstructure. A small addition of Mg allows Al-Ce binary alloy to vary its microstructure as previously received in heat treated Al-Ce binary alloy by sacrificing some mechanical properties such as elongation percentage [8].

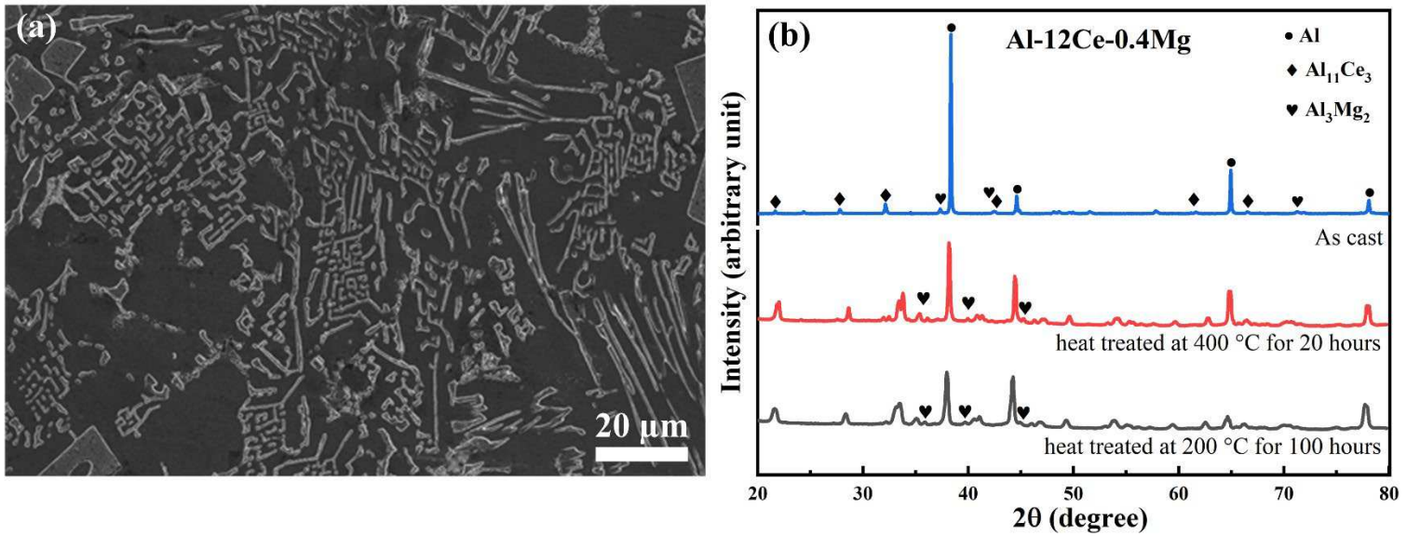

Figure 7: (a) FESEM micrograph of as-cast Al-12Ce-0.4Mg (wt. %) alloy, showing entangled lathe and primary precipitation (parallelogram shape of intermetallic $Al_{11}Ce_3$, (b) XRD pattern

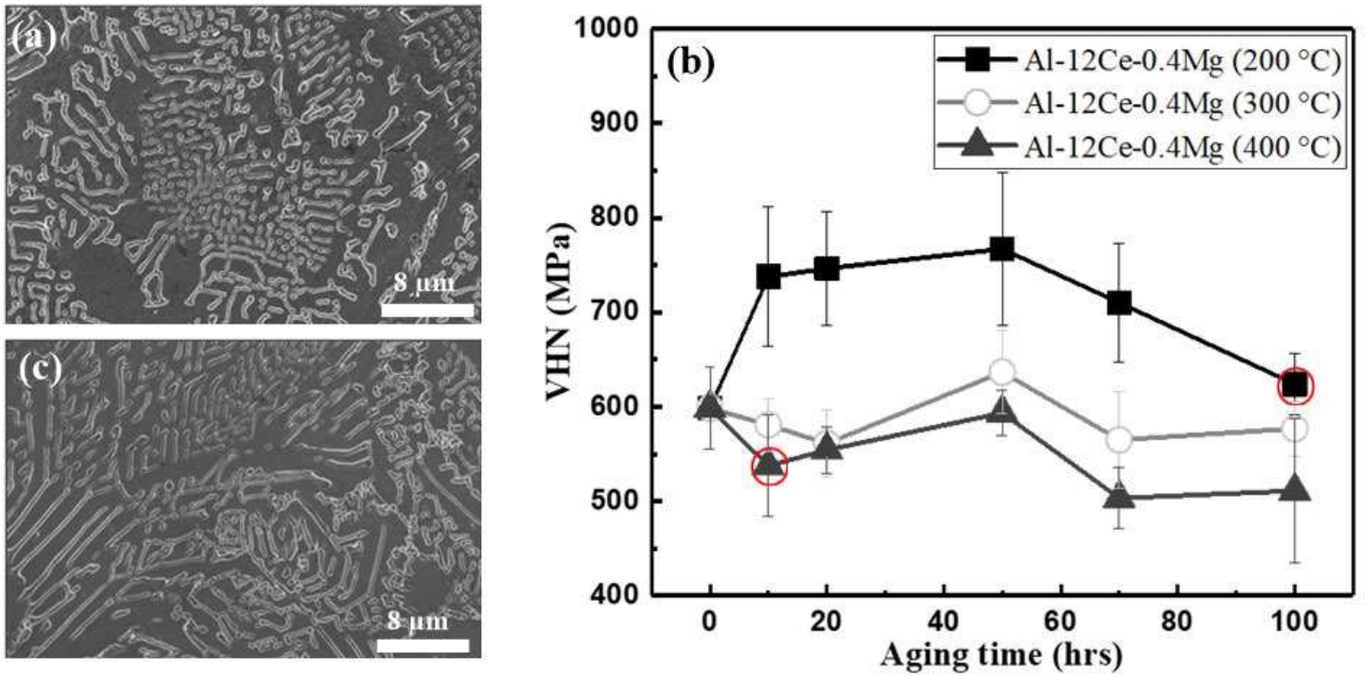

Figure 8: (a) FESEM micrograph showing the lathes of intermetallic converting into spheroids particle by minimizing their strain energy through surface diffusion at 400 °C for 10 hours of aging time (b) Heat treatment study for Al-12Ce-0.4Mg alloy for different time intervals (0, 10, 20, 50, 70 and 100 hours) (c)long lathe-like intermetallic at 200 °C for 100 hours

Table 3: Data for area fraction, aspect ratio and increased strength by Orowan / load transfer/solid solution strengthening mechanisms at a critical point

Alloy	Area fraction of $Al_{11}Ce_3$ (%)	Aspect ratio (length/diameter) of $Al_{11}Ce_3$	Total increment in strength (ΔHV/3) (MPa)	Orowan strengthening Contribution (MPa)	Load transfer + solid solution strengthening contribution (MPa)
Al-12Ce-0.4Mg (after 100 hours of aging time at 200 °C)	23.07 ± 1.23	9.66 ± 9.50	179.23	15.12	164.11
Al-12Ce-0.4Mg (after 10 hours of aging time at 400 °C)	21.67 ± 2.63	4.52 ± 4.65	132.80	18.84	113.96

3.4 Al-12Ce-4Si-0.4Mg alloy

Literature reported that the addition of Si adversely affects the fluidity Al-Si alloy [8]. Therefore, a small amount of Si was added to the Al-Ce alloys. Addition of 4 wt.% Si and 0.4 wt.% Mg to binary Al-12Ce alloy leads to the formation of intermetallic $Al_{11}Ce_3$ due to AlCeSi, as shown in figure 9a. XRD pattern in figure 9b confirms the presence of these phases and is supported by the previous studies [8,9]. XRD pattern at different critical points did not show any additional peaks as cast condition indicates the absence of bulk phase transformation (Figure 9b). After the heat treatment, some critical points (encircled) were selected for microstructural study based on high hardness variation. Figures 10a and b show the micrograph of cast Al-12Ce-4Si-0.4Mg alloy at 200 °C and 400 °C, respectively, after 10 hours of heat treatment. Figure 10c shows the heat treatment analysis of Al-12Ce-4Si-0.4Mg alloy. Heat treatment at high temperature (400 °C) results in fragmentation of $Al_{11}Ce_3$ intermetallic lathe and transformation into particle-like morphology. Hardness improves by 33 % at 200 ° C for 10 hours of aging time compared to as-cast condition (Figure 10c). This increase in hardness was associated with the combined effect of Si and Mg. The decrease in hardness at 400 °C could be expected due to the loss in solid solution strengthening at high temperature and inactivation of the load-carrying capacity of the microstructure due to fragmentation (Figure 10b).

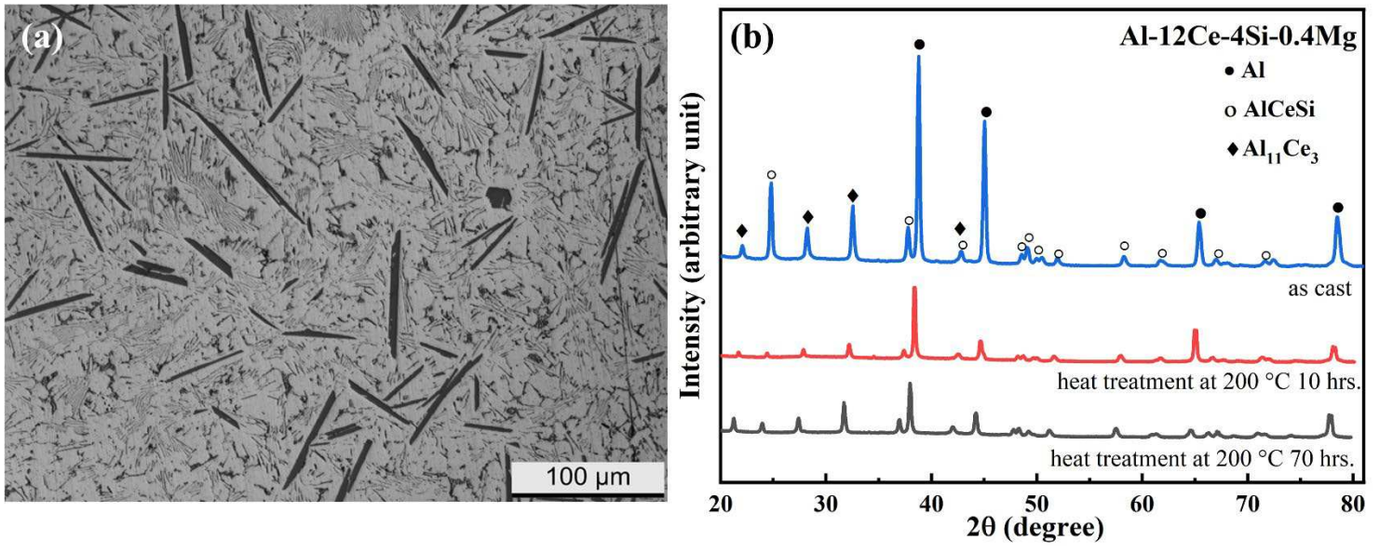

Figure 9: (a) FESEM micrograph of as-cast Al-12Ce-4Si-0.4Mg (wt. %) alloy showing homogeneously distributed eutectic of Al and Al_9Si intermetallic and dispersed intermetallic AlCeSi (b) XRD pattern.

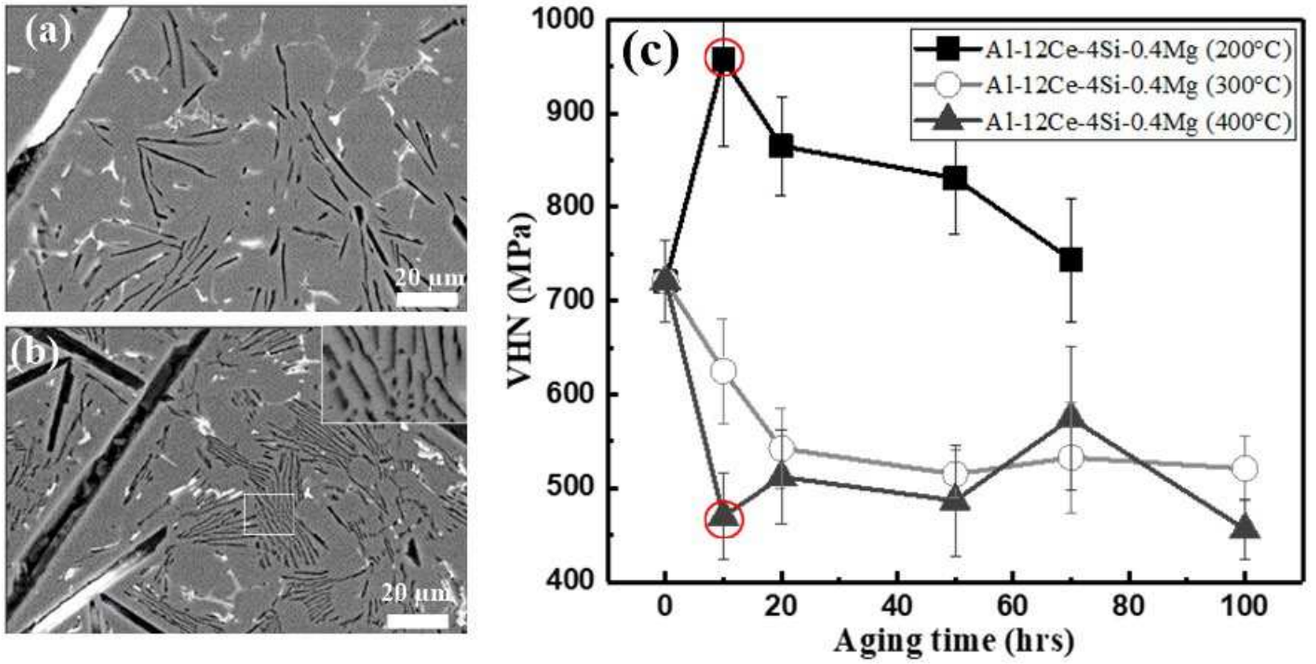

Figure 10: FESEM micrograph of as-cast Al-12Ce-4Si-0.4Mg (wt.%) alloy showing (a) eutectic and intermetallic AlCeSi after 10 hours of aging at 200 °C, (b) fine and spheroid eutectic after 10 hours of heat treatment at 400 °C, (c) Heat treatment of Al-12Ce-4Si-0.4Mg alloy for different time intervals (0, 10, 20, 50, 70 and 100 hours)

3.5 Al-12Ce-4Si-0.4Mg-0.25Sr alloy

Figure 11a demonstrates that further addition of Sr to quaternary alloy refines intermetallic AlCeSi. It changes the AlCeSi aspect ratio from 14.2 ± 4.8 to 9.8 ± 5.4 µm (Figure 9a and 11a). Some critical points (encircled) were selected based on hardness variation and characterization was done (Figure 11b). Addition of Sr increases the room temperature

strength of the quinary alloy as compared the others developed alloys (Figure 11c). An increase in the hardness possibly due to increment in solid solution strengthening by addition of Sr. Figure 11d reported the heat treatment study up to 100 hours for quinary alloy. After 10 hours of heat treatment, a significant reduction in hardness was observed at 200 °C. Quinary alloy is characterized by multiple phases, thus making the analysis challenging. Continuous hardness reduction was seen at 400 °C after a long heat treatment duration, which could be attributed to the minimal contribution of the solid solution strengthening mechanism at high temperatures. The lathes of $Al_{11}Ce_3$ and AlCeSi were smaller and less entangled than in earlier microstructure studies. As a result, the intermetallic phases have a lower load transfer capability than ternary alloys. Therefore, the combined addition of all these mechanisms leads to reducing the hardness.

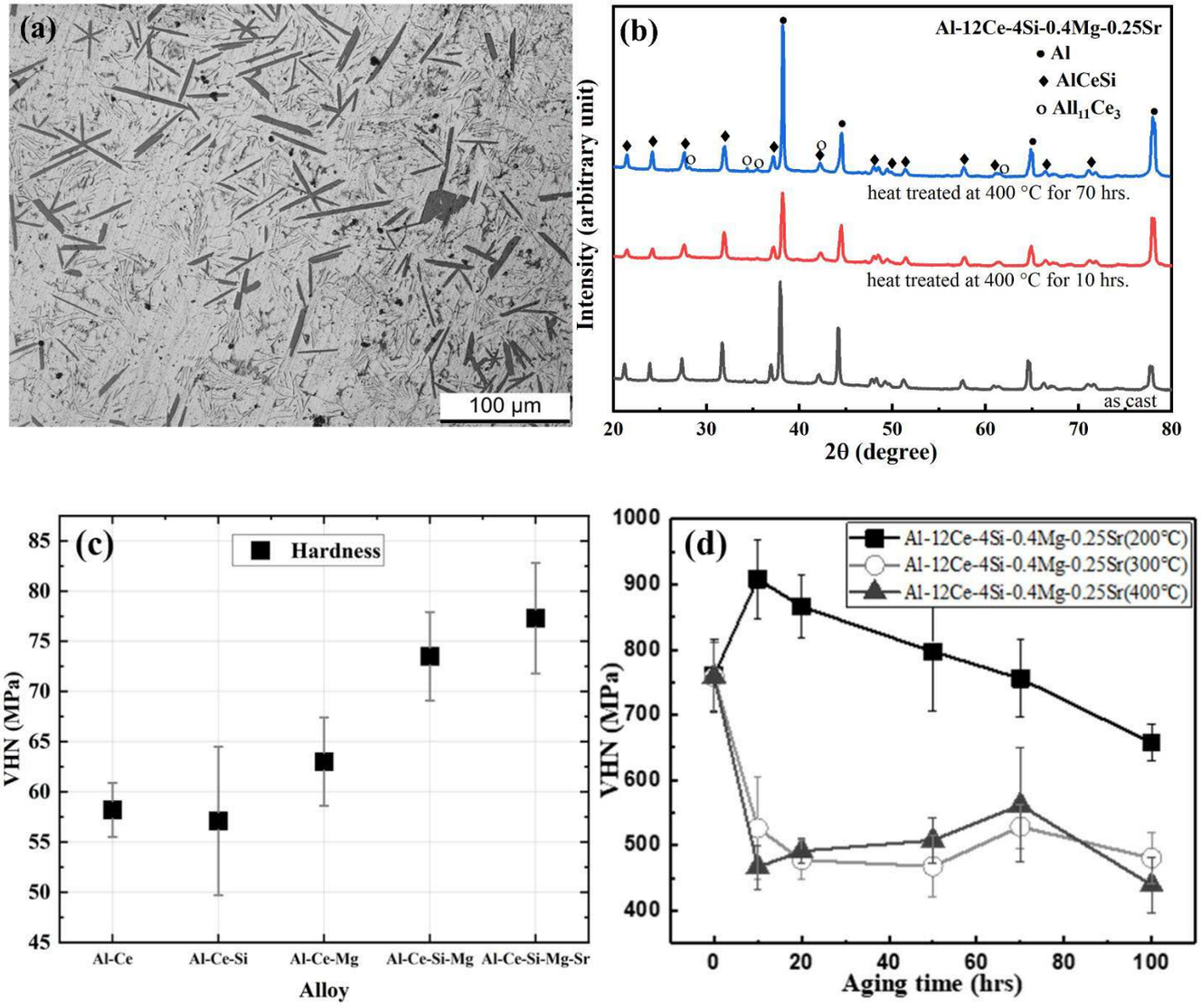

Figure 11: (a) FESEM micrograph of as-cast Al-12Ce-4Si-0.4Mg-0.25Sr alloy, (b) XRD pattern, (c) Hardness comparison plot foe developed alloys (d) Heat treatment study for Al-12Ce-4Si-0.4Mg-0.25Sr alloy for different time intervals (0, 10, 20, 50, 70 and 100 hours)

4. Future work

The Al-Ce-based alloy is a potential heat-resistant aluminum alloy. Tensile strength is intrinsically related to hardness. However, microhardness is only one aspect of the mechanical properties of materials, which cannot replace other mechanical properties tested at high temperatures. In particular, the fatigue strength creeps resistance is also a key parameter in material properties that can be discussed in the future.

5. Conclusions

Microstructure stability of five different Al-Ce based alloys was studied after heat treatment at three different temperatures, i.e., 200 °C, 300 °C and 400 °C. Microhardness measurements were used to ascertain microstructure stability and strengthening mechanisms were discussed. The major conclusions from work are as follows:

1) Al-Ce binary alloys show thermal stability at all the temperatures studied (200 – 400 ° C) due to higher stability of $Al_{11}Ce_3$ intermetallic.
2) Al-12Ce-4Si is thermally stable at in the temperature range of 200-400 C, Due to the presence of thermally stable $Al_{11}Ce_3$ and AlCeSi intermetallic phases.
3) Al-12Ce-0.4Mg and Al-12Ce-4Si-0.4Mg show thermal stability at 200 °C and 300 °C. The strengthening mechanisms involved are solid solution strengthening, load transfer, and Orowan strengthening.
4) The addition of Sr to Al-12Ce-4Si-0.4Mg alloy fragmented the AlCeSi intermetallic and enhanced the room temperature strength. Heat treatment at higher temperatures results in a significant reduction in hardness.

Authorship contribution statement

Dheeraj Kumar Saini: Writing original draft. **Rahul Gope:** Data collection. **Animesh Mandal:** Conceptualization, supervision, writing- review and editing.

References

[1] K.E. Knipling, D.C. Dunand, D.N. Seidman, Int. J. Mater. Res. 97 (2006) 246–265.

[2] Z.C. Sims, D. Weiss, S.K. McCall, M.A. McGuire, R.T. Ott, T. Geer, O. Rios, P.A.E. Turchi, Jom 68 (2016) 1940–1947.

[3] D. Weiss, J. Mater. Eng. Perform. 28 (2019) 1903–1908.

[4] B. Hu, B. Quan, D. Li, X. Wang, Z. Li, X. Zeng, Mater. Sci. Eng. A 812 (2021).

[5] T. Wu, A. Plotkowski, A. Shyam, D.C. Dunand, Mater. Sci. Eng. A 833 (2022) 142551.

[6] D.R. Manca, A.Y. Churyumov, A. V. Pozdniakov, A.S. Prosviryakov, D.K. Ryabov, A.Y. Krokhin, V.A. Korolev, D.K. Daubarayte, Met. Mater. Int. 25 (2019) 633–640.

[7] Y. Liu, R.A. Michi, D.C. Dunand, Mater. Sci. Eng. A 767 (2019).

[8] D. Weiss, Adv. Cast. Technol. (2018).

[9] Z.C. Sims, O.R. Rios, D. Weiss, P.E.A. Turchi, A. Perron, J.R.I. Lee, T.T. Li, J.A. Hammons, M. Bagge-Hansen, T.M. Willey, K. An, Y. Chen, A.H. King, S.K. McCall, Mater. Horizons 4 (2017) 1070–1078.

[10] M.C. Gao, N. Ünlü, G.J. Shiflet, M. Mihalkovic, M. Widom, (n.d.).

[11] Y. Du, Y.A. Chang, B. Huang, W. Gong, Z. Jin, H. Xu, Z. Yuan, Y. Liu, Y. He, F.Y. Xie, Mater. Sci. Eng. A 363 (2003) 140–151.

[12] A. De Luca, D.C. Dunand, D.N. Seidman, Acta Mater. 144 (2018) 80–91.

[13] Hirsch, PB, F.J. Humphreys, The Physics and Strength of Plasticity, A. Argon, 1969.

[14] W.L. Fink, J. Appl. Phys. 13 (1942) 75–83.

[15] E. Nembach, 17 (1997) 57590.

[16] J.H. Westbrook, R.L. Fleischer, (1995) 1995.

[17] M.A. Meyers, K.K. Chawla, (1984) 221.

[18] H. Frost, M.F. Ashby, Deformation Mechanism Maps: The Plasticity and Creep of Metals and Ceramics, Pergamon press, n.d.

[19] P. Zhang, S.X. Li, Z.F. Zhang, Mater. Sci. Eng. A 529 (2011) 62–73.

[20] E.T. Stromme, H.B. Henderson, Z.C. Sims, M.S. Kesler, D. Weiss, R.T. Ott, F. Meng, S. Kassoumeh, J. Evangelista, G. Begley, O. Rios, Jom 70 (2018) 866–871.

[21] S. Dais, R. Messer, A. Seeger, Mater. Sci. Forum 15–18 (1987) 419–424.

[22] S. Illman, J. Math. Sci. 105 (2001) 1843–1847.

[23] R. Abbaschian, R. E, Physical Metallurgy Principles-SI Version, 2009.

[24] D.N. Seidman, E.A. Marquis, D.C. Dunand, Acta Mater. 50 (2002) 4021–4035.

[25] C. Weiping, J. Mater. Sci. Lett. 16 (1997) 1824–1826.